Cancer Cell, Volume *41*

Supplemental information

Lineage tracing reveals clonal progenitors and long-term persistence of tumor-specific T cells during immune checkpoint blockade

Joy A. Pai, Matthew D. Hellmann, Jennifer L. Sauter, Marissa Mattar, Hira Rizvi, Hyung Jun Woo, Nisargbhai Shah, Evelyn M. Nguyen, Fathema Z. Uddin, Alvaro Quintanal-Villalonga, Joseph M. Chan, Parvathy Manoj, Viola Allaj, Marina K. Baine, Umesh K. Bhanot, Mala Jain, Irina Linkov, Fanli Meng, David Brown, Jamie E. Chaft, Andrew J. Plodkowski, Mathieu Gigoux, Helen H. Won, Triparna Sen, Daniel K. Wells, Mark T.A. Donoghue, Elisa de Stanchina, Jedd D. Wolchok, Brian Loomis, Taha Merghoub, Charles M. Rudin, Andrew Chow, and Ansuman T. Satpathy

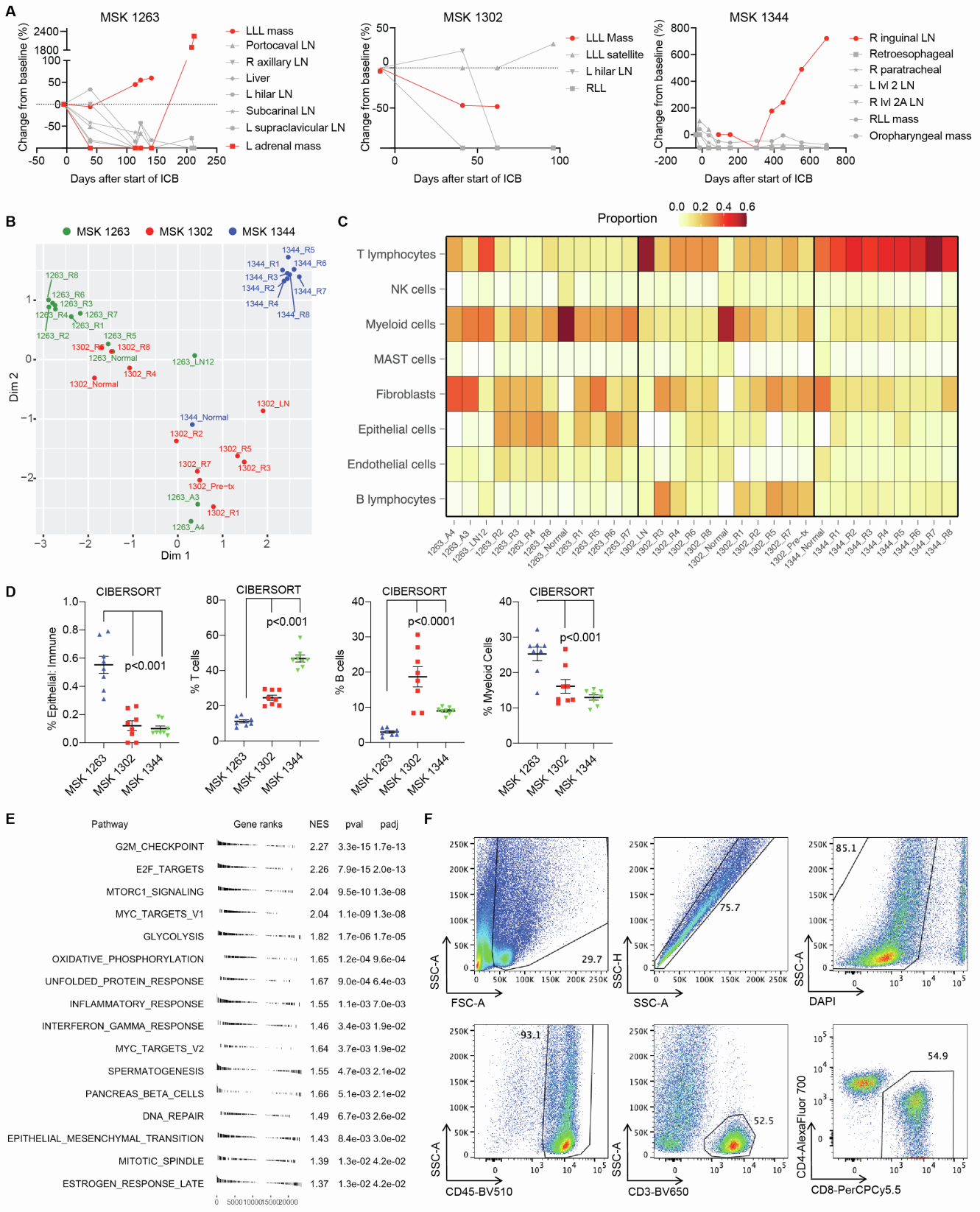

Figure S1. Regional bulk transcriptional heterogeneity in resections after ICB. Related to Figure 1.

A) Quantification of surface area of individuals lesions on radiographical studies over time normalized to baseline lesion size in three patients. Red lines indicate lesions that were resected and analyzed in this study.
B) Principal component analysis of bulk RNA sequencing of regions from three patients undergoing oligometastatic resections.
C) Heat map of CIBERSORT quantification of various immune populations (y axis) across the different regions from three patients (x axis).
D) Percentage of cells in various immune populations as quantified by CIBERSORT. Each point represents one region. Error bars represent standard error of the mean.
E) GSEA of pathways differentially expressed among viable vs. no viable tumor regions as measured by bulk RNA-seq.
F) Representative gating strategy for the isolation of $CD3^+$ T cells by flow cytometry.

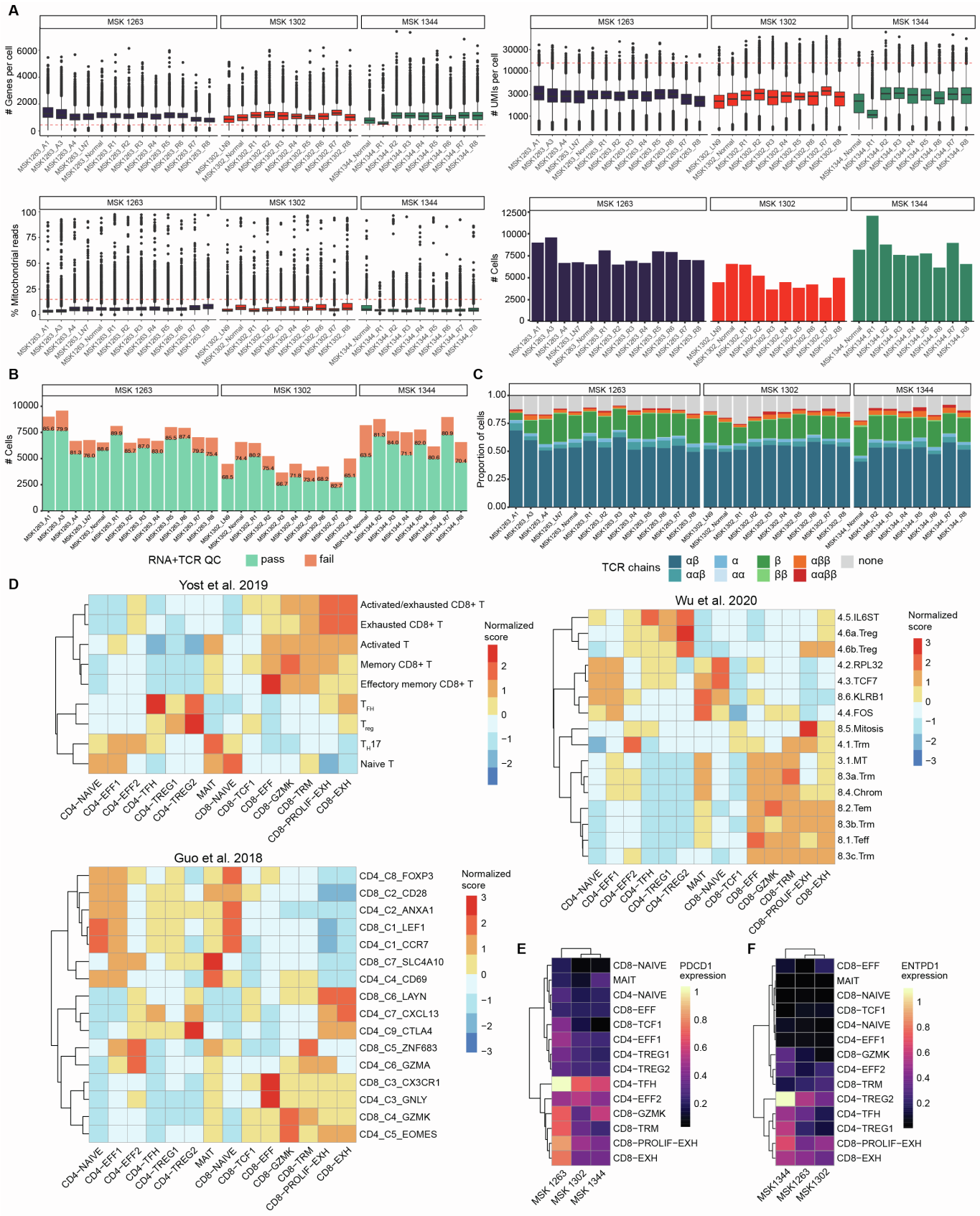

Figure S2. Quality control and comparison of cluster-defining genes to published scRNA-seq clusters. Related to Figure 1.

A) Box and whisker plots of number of genes detected per cell, number of unique molecular identifiers (UMIs) per cell, percent mitochondrial reads per cell, and number of cells captured per region undergoing scRNA/TCR-seq. Cutoffs used for quality filtering are shown as dotted red lines. Box and whisker plots are defined as: center line, median; box, interquartile range; upper whisker limit, maximum without outliers; lower whisker limit; minimum without outliers; points, outliers.
B) Bar plot of absolute number of cells passing (green) and failing (orange) QC per region undergoing scRNA/TCR-seq. Numbers indicate percentage of cells in library passing QC.
C) Bar plot of absolute number of cells for which TCRα only (light blue), TCRβ only (green), or both TCRα and TCRβ chains (teal) were reconstructed per region undergoing scRNA/TCR-seq. T cells for which multiple TCRβ chains were captured (light green, orange, red) were excluded from further analysis.
D) Heat map comparing clusters designated in our dataset (x axis) and clusters designated in the indicated external scRNA-seq datasets (y axis). Color scale represents external cluster gene scores computed per cell in our dataset and normalized per row.
E) *PDCD1* expression of cells in each cluster from each patient.
F) *ENTPD1* expression of cells in each cluster from each patient.

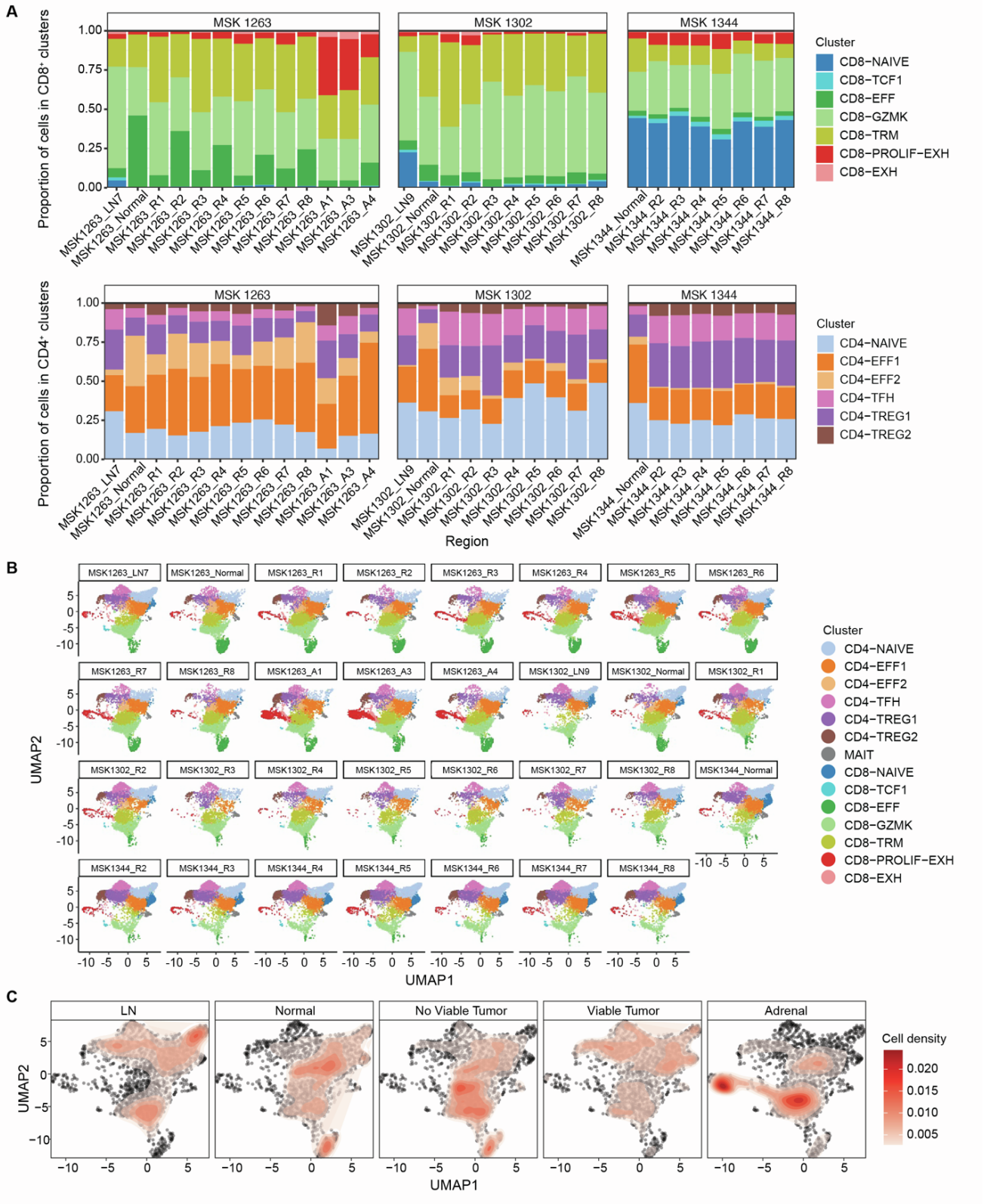

Figure S3. Cluster representation across patients. Related to Figure 1.
A) Bar plots of the proportion of cells in the indicated clusters among CD8$^+$ T cells (top) or CD4$^+$ T cells (bottom) per region undergoing scRNA-seq.
B) UMAP of cluster representation across the 31 regions undergoing scRNA/TCR-seq that passed QC.
C) UMAP of sorted CD3$^+$ T cells among each region type colored by cell density.

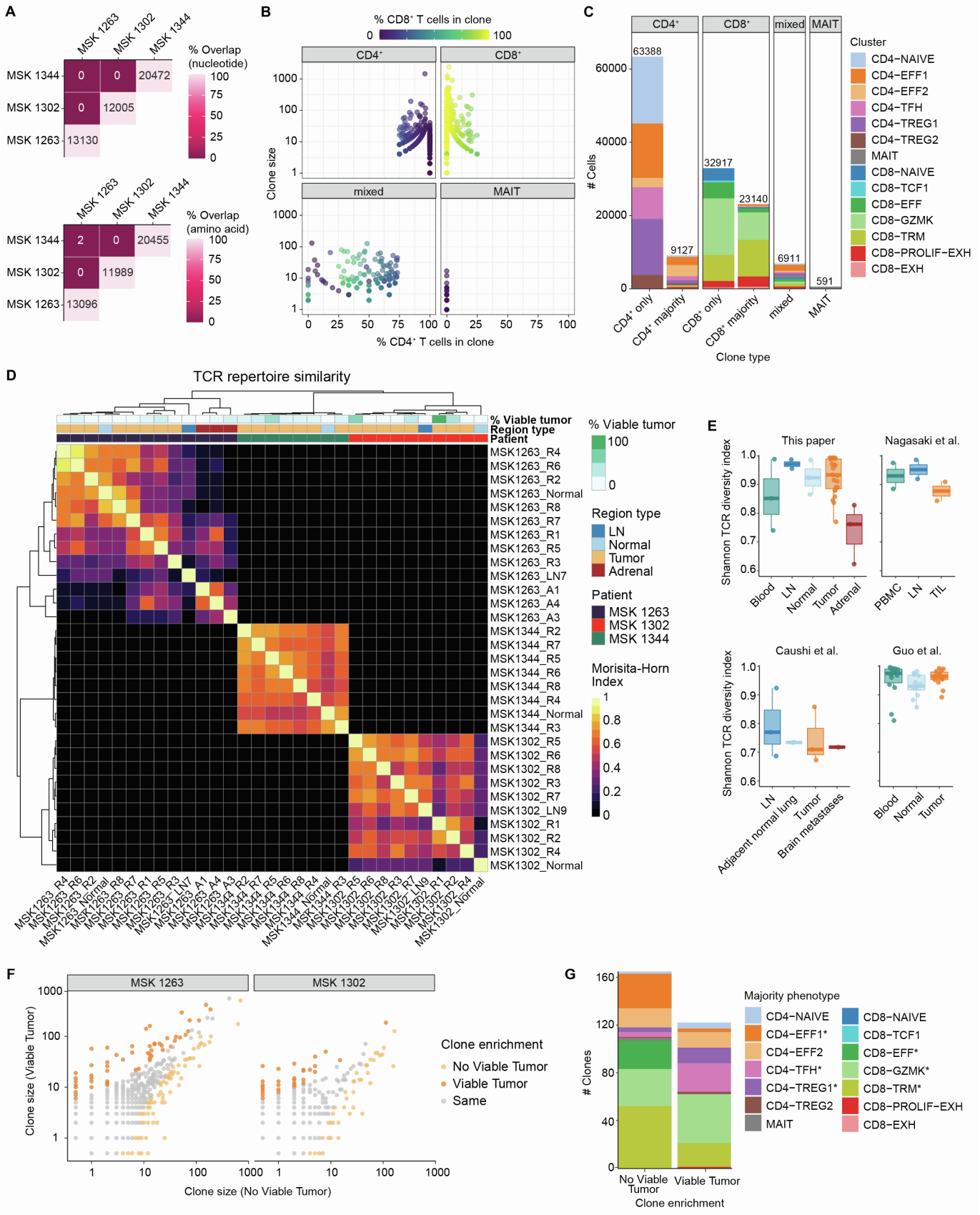

Figure S4. TCR repertoire similarity and diversity. Related to Figure 1.

A) Heat map of TCR clonal overlap between patients based on CDR3αβ nucleotide (top) or amino acid (bottom) sequence.
B) Scatterplot of percent $CD4^+$ T cells in each clone versus clone size among clones in each clone designation ($CD8^+$, $CD4^+$, mixed, or MAIT). Each point represents one TCRαβ clone and is colored by the percentage of $CD8^+$ cells in the clone.
C) Bar plots of cells within each clone type colored by phenotype cluster.
D) Morisita-Horn Index of TCRαβ repertoire similarity among different regions (minimum clone size = 10).
E) TCR repertoire diversity of each region type as measured by normalized Shannon index. Data is from the tissue sorted $CD3^+$ scRNA/TCR-seq dataset and three external datasets[16,30,31] of samples from lung cancer patients. Box and whisker plots are defined as: center line, median; box, interquartile range; upper whisker limit, maximum without outliers; lower whisker limit; minimum without outliers; points, outliers.
F) Scatterplot of the number of cells in regions with no viable tumor vs. regions with viable tumor per clone. Each point represents one clone classified as enriched in viable tumor (dark orange) or no viable tumor (light orange) regions (Fisher's exact test, $p<0.05$).
G) Bar plot of clones enriched in no viable tumor regions or viable tumor regions, colored by majority phenotype within each clone. (* denotes significance as determined by Fisher's exact test, $p<0.05$).

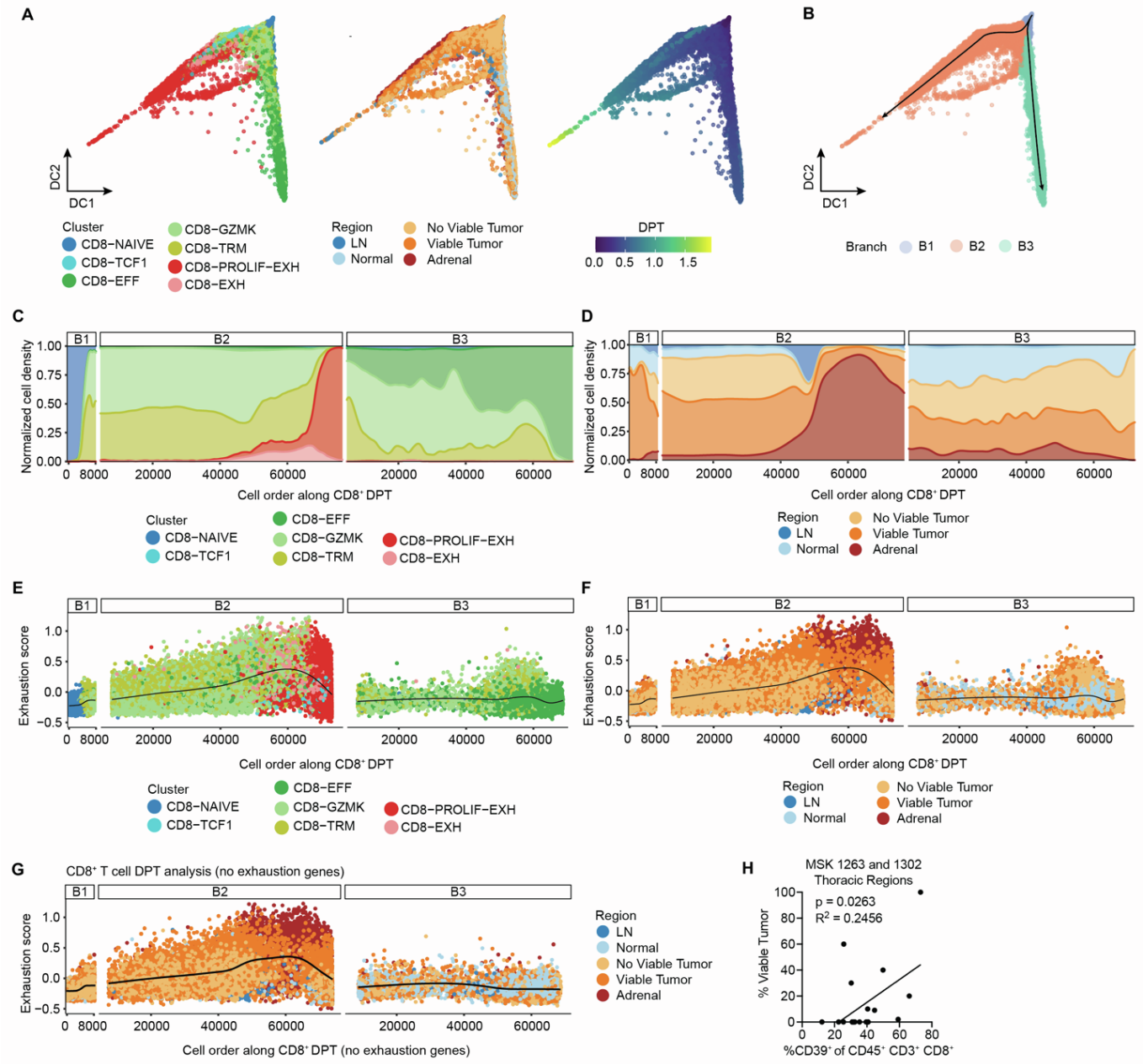

Figure S5. Diffusion analysis of CD8⁺ T cell clones. Related to Figure 1.

A) Diffusion map of cells from CD8⁺ T cell clones colored by phenotype cluster (left), region type (center), or diffusion pseudotime (DPT) (right).

B) Diffusion map of cells from CD8⁺ T cell clones colored by DPT branch.

C-D) Density plots of cell phenotypes (C) or region type (D) along DPT branches B1, B2, and B3.

E-F) Scatter plot of exhaustion scores among CD8⁺ T cells ordered along DPT branches B1, B2, and B3. Points are colored by CD8⁺ phenotype cluster (E) or region type (F).

G) Scatter plot of exhaustion scores among CD8⁺ T cells ordered along DPT branches B1, B2, and B3 calculated without genes in the exhaustion signature. Points are colored by region type.

H) Correlation of % CD8⁺ T cells expressing CD39 and % viable tumor per region from MSK 1263 and 1302.

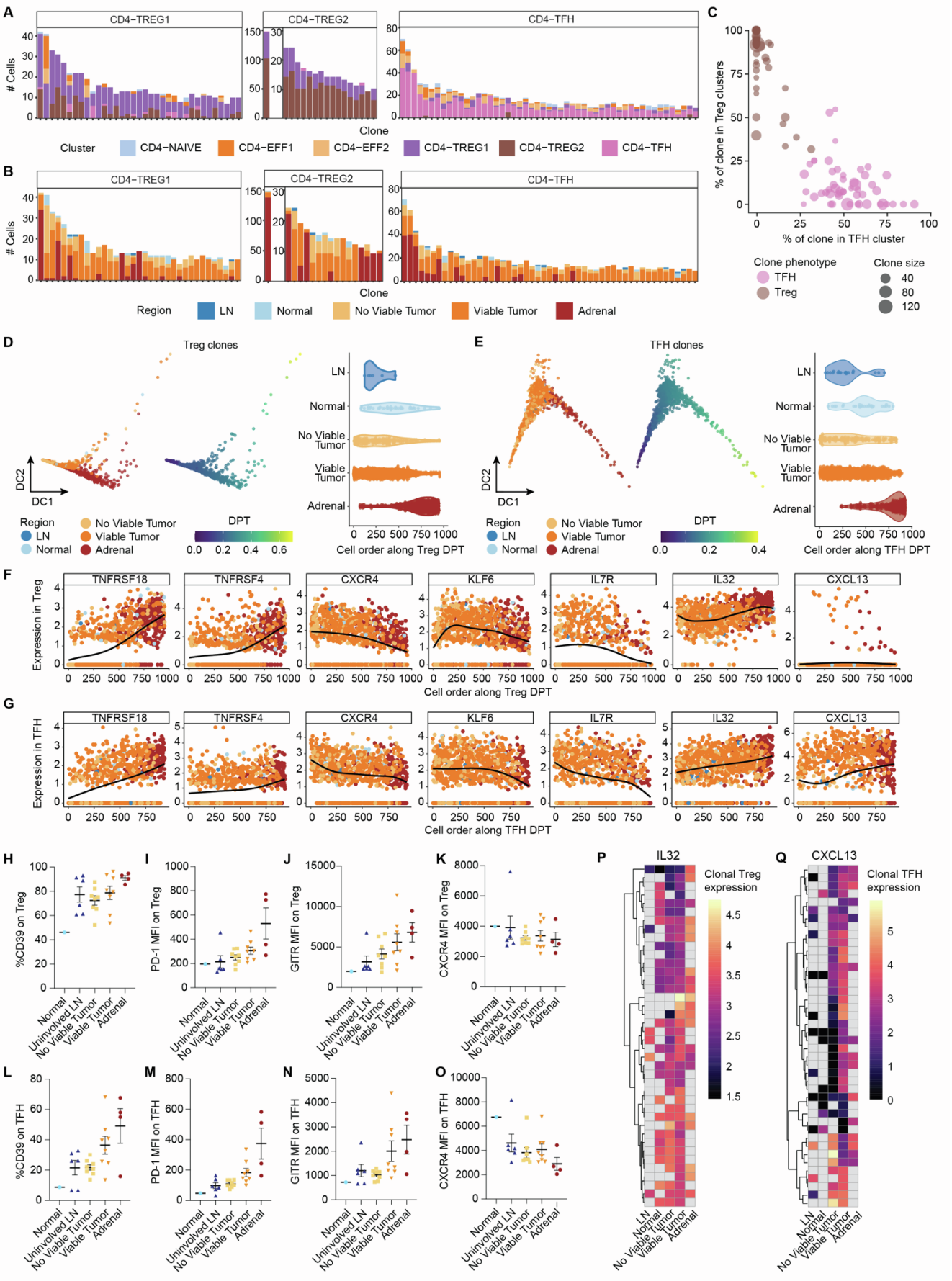
A
CD4−TREG1
CD4−TREG2
CD4−TFH
Cells
Clone
Cluster
CD4−NAIVE
CD4−EFF1
CD4−EFF2
CD4−TREG1
CD4−TREG2
CD4−TFH
B
Region
LN
Normal
No Viable Tumor
Viable Tumor
Adrenal
C
% of clone in Treg clusters
% of clone in TFH cluster
Clone phenotype
TFH
Treg
Clone size
D
Treg clones
DC2
DC1
DPT
Cell order along Treg DPT
E
TFH clones
Cell order along TFH DPT
F
TNFRSF18
TNFRSF4
CXCR4
KLF6
IL7R
IL32
CXCL13
Expression in Treg
G
Expression in TFH
H
%CD39 on Treg
I
PD-1 MFI on Treg
J
GITR MFI on Treg
K
CXCR4 MFI on Treg
L
%CD39 on TFH
M
PD-1 MFI on TFH
N
GITR MFI on TFH
O
CXCR4 MFI on TFH
P
IL32
Clonal Treg expression
Q
CXCL13
Clonal TFH expression

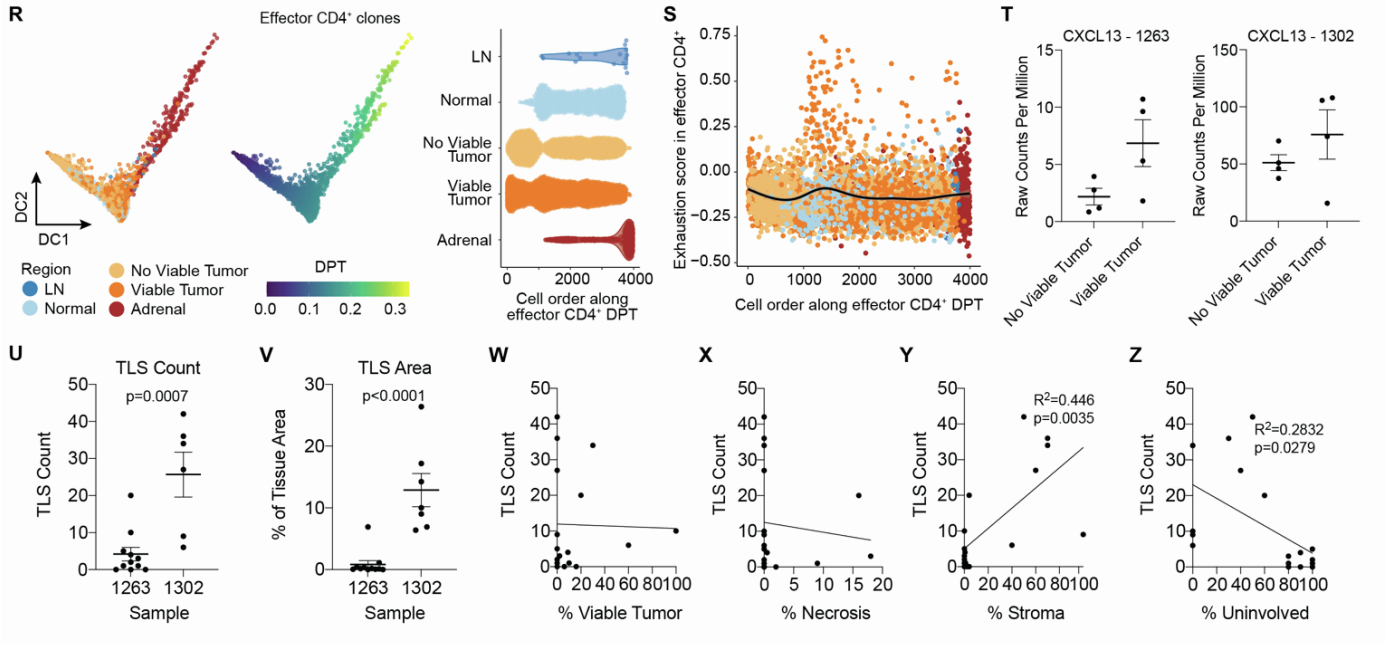

Figure S6. Diffusion analysis of Treg, TFH, and effector CD4⁺ T cell clones. Related to Figure 1.

A-B) Phenotype (A) and regional (B) composition of Treg and TFH clones expanded >10 cells from MSK 1263, 1302, and 1344.

C) Scatterplot of phenotypic overlap between TFH and Treg clones. Each dot representing one clone is colored by the clone phenotype assigned by majority cluster and sized according to clone size.

D-E) Diffusion map of cells from Treg (D) or TFH (E) clones with clone size >10 cells colored by region type (left) or DPT (center). Beeswarm plot of cells ordered by DPT grouped by region type (right).

F-G) Expression changes of select top DC1-varying genes among Treg (F) or TFH (G) cells ordered along DPT and colored by region type as in (D) and (E).

H-K) Flow cytometric quantification of %CD39 (H), PD-1 MFI (I), GITR MFI (J), and CXCR4 MFI (K) on Treg cells across the indicated region types. Error bars represent standard error of the mean.

L-O) Flow cytometric quantification of %CD39 (L), PD-1 MFI (M), GITR MFI (N), and CXCR4 MFI (O) on TFH cells across the indicated region types. Error bars represent standard error of the mean.

P) Heatmap of *IL32* expression among Treg clones present in at least two region types.

Q) Heatmap of *CXCL13* expression among TFH clones present in at least two region types.

R) Diffusion map of cells from effector CD4⁺ T cell clones (CD4-EFF1 and CD4-EFF2 clusters) with clone size >10 cells colored by region type (left) or DPT (center). Beeswarm plot of cells ordered by DPT grouped by region type (right).

S) Scatter plot of exhaustion scores among effector CD4⁺ cells ordered along the DPT. Points are colored by region type as in (R).

T) Quantification of transcriptomic levels of *CXCL13* by bulk RNA-seq (see also **Fig S1**) of regions without and with viable tumor. Error bars represent standard error of the mean.

U) TLS count was performed by automated counting by Halo software (see **Methods**). Statistical testing by student's t-test. Error bars represent standard error of the mean.

V) TLS area was calculated by expressing the surface area of TLSs (automated annotation by Halo) as percent of tissue area. Statistical testing by student's t-test. Error bars represent standard error of the mean.

W-Z) Linear correlation per region of TLS count and percent viable tumor (W), necrosis (X), stroma (Y), and uninvolved (Z).


A
CD8⁺ T cell clones in tumor regions
Clones
Clonal exhaustion score
B
MSK1263
MSK1302
40
90 clones
23
25 clones
Clone has LN cell in cluster 2: Progenitor exhausted
Yes
No
C
LN
Tumor
Clones
% of clone in cluster 2: Progenitor exhausted
D
Top expanded exhausted CD8⁺ clones found in LN and tumor
Proportion of cells in region
Re-clustered
1: Central memory
2: Progenitor exhausted
3: TRM
4: Tox^high exhausted
5: PD−1^high exhausted
6: TIM−3^high exhausted
7: Proliferating exhausted
Original cluster
CD8−NAIVE
CD8−EFF
CD8−GZMK
CD8−TRM
CD8−PROLIF−EXH
CD8−EXH
E
LN cells in exhausted CD8⁺ clones
Clones
Clonal TCF7 expression
F
CD8⁺ clones in CD8-EXH and CD8-PROLIF-EXH
MSK 1263 Thoracic
MSK 1263 Adrenal
MSK 1302
13
227 clones
12
115 clones
3
41 clones
LN TCF7^high status
TCR match in LN, TCF7 > 0
TCR match in LN, TCF7 = 0
no TCR match in LN
G
LN cells in exhausted CD8⁺ clones
Clones
Clonal progenitor score
H
Exhaustion^hi CD8⁺ clones
MSK 1263 Thoracic
MSK 1263 Adrenal
MSK 1302
8
462 clones
5
173 clones
6
177 clones
I
Exhaustion^hi CD8⁺ clones (Caushi et al. 2021)
MD01-004
MD01-005
MD043-011
8
148 clones
20
203 clones
28
453 clones
J
Exhaustion^hi CD8⁺ clones (Nagasaki et al. 2022)
LC01
LC03
1
31 clones
19
102 clones
K
TFH DE: LN vs. Tumor
−log10(adjusted p-value)
Average log2(fold change)
Region
LN
Tumor
DUSP4
CREM
JUNB
RGCC
SARAF
ZFP36
MCL1
ZNF331
TPT1
KLF6
TNFAIP3
BTG1
RGS1
CXCR4
YPEL5
SRGN
TSC22D3
LIMD2
MTRNR2L12
IL16
CHI3L2
VIM
ID3
SELL
AREG
PTPRC
PDCD1
NR4A2
TCF7
MALAT1
CTLA4
CCL5
HSPA1A
CD79A
L
Treg DE: LN vs. Tumor
−log10(adjusted p-value)
Average log2(fold change)
Region
LN
Tumor
HSPA1B
HSP90AA1
HSPA1A
DUSP4
ARHGDIB
H3F3B
VIM
ZFP36
DNAJB1
MYL6
HSP90AB1
RPL36AL
LDHA
CREM
HSPH1
MALAT1
RPS24
PCBP1
MTRNR2L12
FTH1
TENT5C
CHI3L2
LMNA
IFITM1
RPS2
LGALS1
SH2D2A
BAG3
CDKN1A
SOCS1
KIAA1551
ZFAND2A
MYADM
MTRNR2L8
MAL
LINC02195
ANXA1
CCL4
LAG3
JUN
CRIP1
EEF1G
M
Top expanded TFH clones found in LN and tumor
Proportion of cells in region
Cluster
CD4−NAIVE
CD4−EFF1
CD4−EFF2
CD4−TFH
CD4−TREG1
CD4−TREG2
N
Top expanded Treg clones found in LN and tumor
Proportion of cells in region

Figure S7. Identification of LN progenitor states. Related to Figure 2.
A) Distribution of average exhaustion score among $CD8^+$ T cell clones in tumor tissue regions. Clones with an average exhaustion score >0 were defined as $CD8^+$ T cell clones with high exhaustion scores ($exhaustion^{hi}$).
B) Proportion of expanded $exhausted^{hi}$ $CD8^+$ T clones shared between the LN and tumor with LN cells in progenitor exhausted cluster 2.
C) Histograms showing the percentage of cells per clone in progenitor exhausted cluster 2 among the LN and tumor compartments.
D) Bar plots of phenotype composition within each region for top expanded $exhaustion^{hi}$ $CD8^+$ T cell clones that could be found in both the LN and tumor regions. Bars are colored by re-clustered (top) or original total T cell population (bottom) cluster.
E) Distribution of average *TCF7* expression among $CD8^+$ T cell clones in LN regions.
F) Pie chart of $CD8^+$ T cell clones in the CD8-EXH and CD8-PROLIF-EXH clusters in the tumor that could be matched to a clonotype in the LN (medium blue and dark blue, “TCR match in LN”). Dark blue slice indicates that the matched clone could be found expressing *TCF7* in the LN.
G) Distribution of average progenitor score among $CD8^+$ T cell clones in LN regions. Clones with an average progenitor score >0 were defined as $CD8^+$ T cell clones with a LN progenitor.
H) Pie chart of $exhaustion^{hi}$ $CD8^+$ T cell clones in the tumor that could be matched to a clonotype in the LN (medium blue and dark blue, “TCR match in LN”) in the scRNA/TCR-seq dataset. Dark blue slice indicates that the matched clone could be found expressing *TCF7* in the LN, as in (F).
I-J) Pie chart of $CD8^+$ T cell clones with high exhaustion scores in the tumor that could be matched to a clonotype in the LN (medium blue and dark blue, “TCR match in LN”) based on datasets generated by Caushi et al[30] (I) and Nagasaki et al[31] (J). Dark blue slice indicates that the matched clone could be found expressing *TCF7* in the LN as in (F).
K-L) Volcano plot of differentially expressed genes between clone-matched cells in the LN and tumor from TFH (K) or Treg (L) clones.
M-N) Bar plots of phenotype composition within each region for top expanded TFH (M) or Treg (N) clones that could be found in both the LN and tumor regions. Bars are colored by original total T cell population clustering.

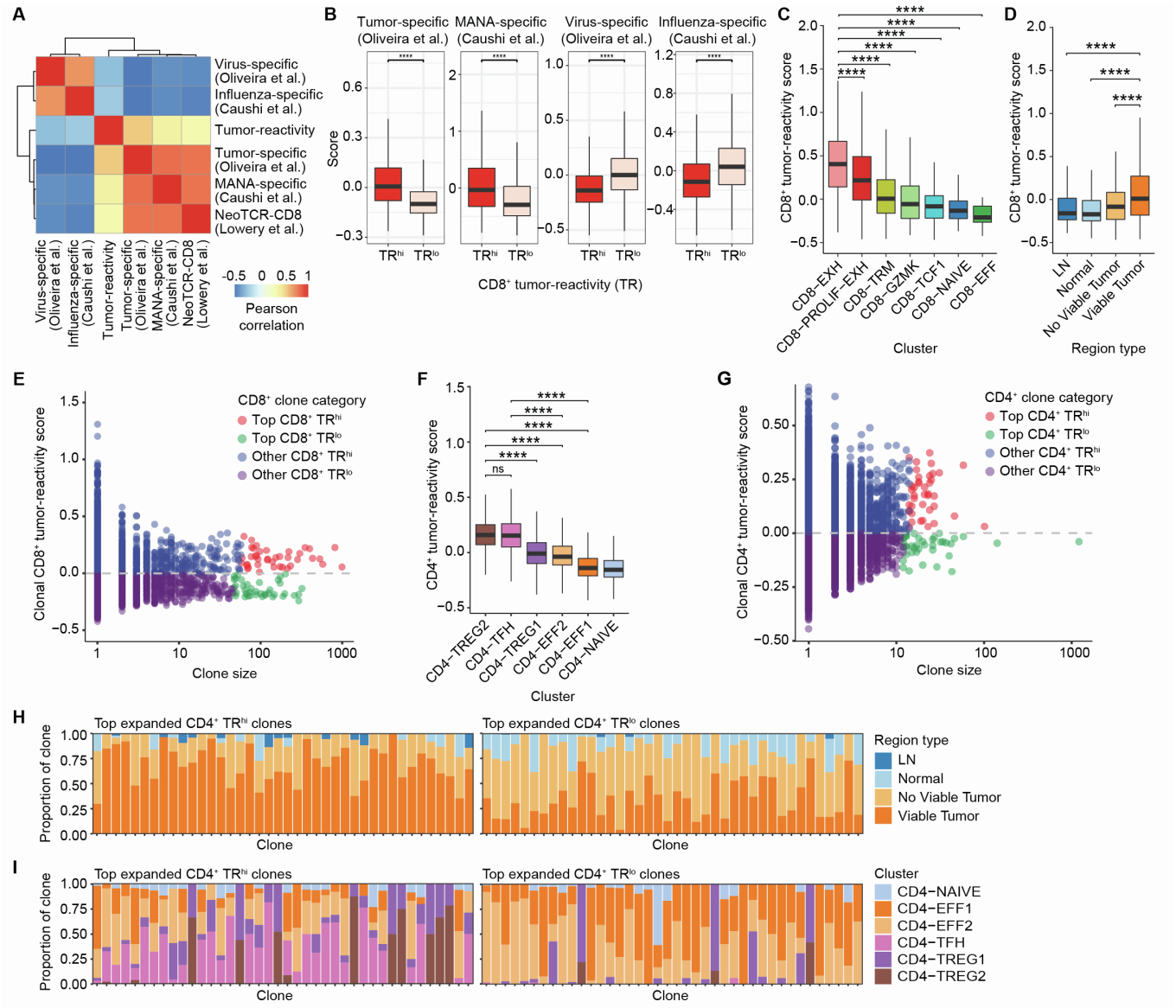

Figure S8. Characterization of TR^{hi} and TR^{lo} CD8$^+$ and CD4$^+$ T cell clones. Related to Figure 3.

A) Heat map of Pearson correlation matrix between CD8$^+$ tumor-reactivity score with 'tumor-specific'[35], 'MANA-specific'[30], 'NeoTCR-CD8'[36], 'virus-specific'[35], and 'influenza-specific'[30] scores computed on all cells.

B) Box and whisker plots of 'tumor-specific'[35], 'MANA-specific'[30], 'virus-specific'[35], and 'influenza-specific'[30] scores among CD8$^+$ T cells with high (>0, TR^{hi}) and low (≤0, TR^{lo}) tumor-reactivity scores. Statistical testing by two-sided t-test (**** <0.0001).

C) Box and whisker plot of tumor-reactivity scores[34] among the indicated CD8$^+$ T cell clusters in MSK 1263, 1302, and 1344. Statistical testing by two-sided t-test (**** <0.0001).

D) Box and whisker plot of CD8$^+$ tumor-reactivity scores across the indicated region types. Statistical testing by two-sided t-test (**** <0.0001).

E, G) Scatterplot of clone size and tumor-reactivity score per CD8$^+$ (E) or CD4$^+$ (G) clone, colored by tumor-reactivity category. 'Top TR^{hi}' and 'top TR^{lo}' represent the 40 most expanded TR^{hi} or TR^{lo} clones, respectively.

F) Box and whisker plot of CD4$^+$ tumor-reactivity scores[36] among the indicated CD4$^+$ T cell clusters in MSK 1263, 1302, and 1344. Statistical testing by two-sided t-test (**** <0.0001).

H-I) Bar plots of the proportion of cells in the indicated region type (H) or phenotypic cluster (I) among the top 40 most expanded TR^{hi} (left) or TR^{lo} (right) $CD4^{+}$ clones.
All box and whisker plots are defined as: center line, median; box, interquartile range; upper whisker limit, maximum without outliers; lower whisker limit; minimum without outliers.

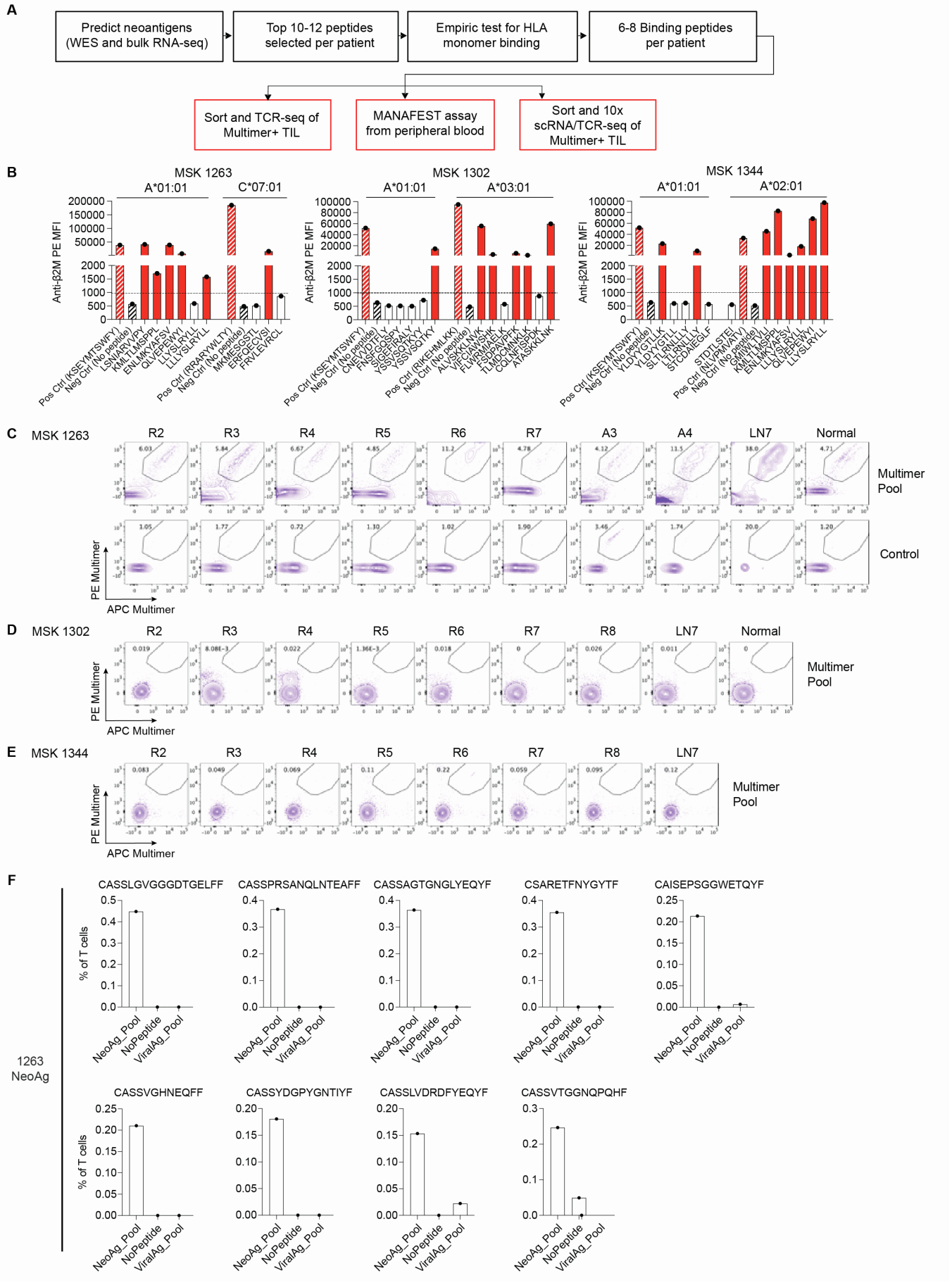
A
Predict neoantigens (WES and bulk RNA-seq)
Top 10-12 peptides selected per patient
Empiric test for HLA monomer binding
6-8 Binding peptides per patient
Sort and TCR-seq of Multimer+ TIL
MANAFEST assay from peripheral blood
Sort and 10x scRNA/TCR-seq of Multimer+ TIL
B
MSK 1263
A*01:01
C*07:01
MSK 1302
A*01:01
A*03:01
MSK 1344
A*01:01
A*02:01
Anti-β2M PE MFI
C
MSK 1263
R2
R3
R4
R5
R6
R7
A3
A4
LN7
Normal
Multimer Pool
Control
PE Multimer
APC Multimer
D
MSK 1302
R2
R3
R4
R5
R6
R7
R8
LN7
Normal
Multimer Pool
PE Multimer
APC Multimer
E
MSK 1344
R2
R3
R4
R5
R6
R7
R8
LN7
Multimer Pool
PE Multimer
APC Multimer
F
1263 NeoAg
CASSLGVGGGDTGELFF
CASSPRSANQLNTEAFF
CASSAGTGNGLYEQYF
CSARETFNYGYTF
CAISEPSGGWETQYF
CASSVGHNEQFF
CASSYDGPYGNTIYF
CASSLVDRDFYEQYF
CASSVTGGNQPQHF
% of T cells
NeoAg_Pool
NoPeptide
ViralAg_Pool

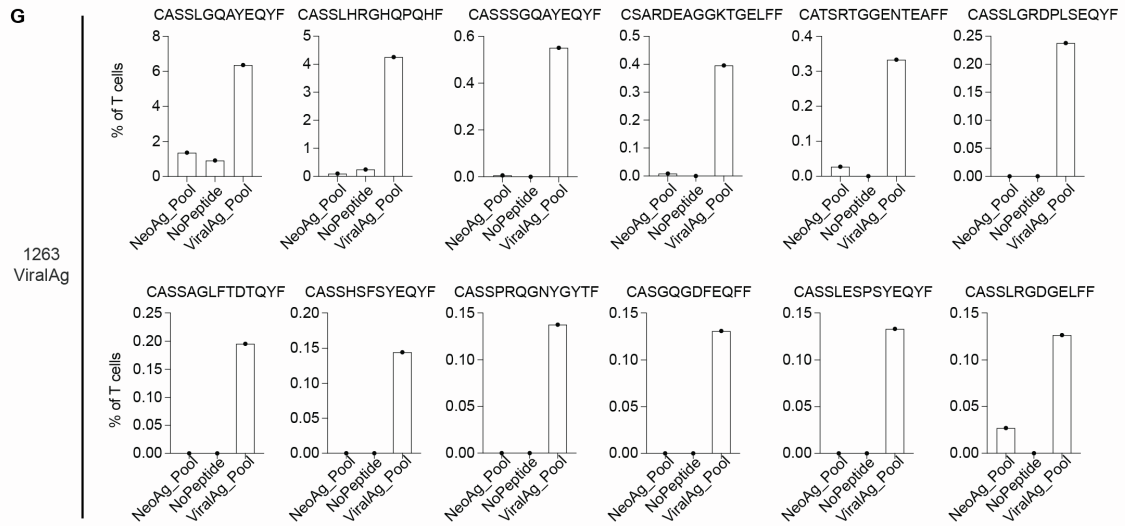

Figure S9. Empirical methods for identifying tumor specificity. Related to Figures 3 and 4.
A) Summary of empirical approaches for identifying tumor-specific TCR clones utilizing tumor-infiltrating lymphocytes (TIL) and peripheral blood.
B) Bar plots of anti-β2M-PE fluorescence on streptavidin-coated beads that were incubated with HLA monomers and peptides utilized in the HLA-peptide binding assay. Control conditions (e.g. positive control and negative control) are indicated by the striped lines. MFI of 1000 was utilized as the cutoff for HLA binding and stabilization by candidate neopeptide. Conditions yielding a PE MFI >1000 are colored in red.
C) Flow cytometry plots of multimer$^+$ populations gated on CD8$^+$ T cells from MSK 1263 tissue TILs cultured with multimer pool or control multimer.
D-E) Flow cytometry plots of multimer$^+$ populations gated on CD8$^+$ T cells from MSK 1302 (D) and MSK 1344 (E) tissue TILs cultured with multimer pool.
F) TCRs (heading indicates CDR3 sequence of TCRβ chain) that elicited preferential reactivity to neoantigen (NeoAg) peptide pool (see **Methods**).
G) TCRs (heading indicates CDR3 sequence of TCRβ chain) that elicited preferential reactivity to viral antigen (ViralAg) peptide pool (see **Methods**).

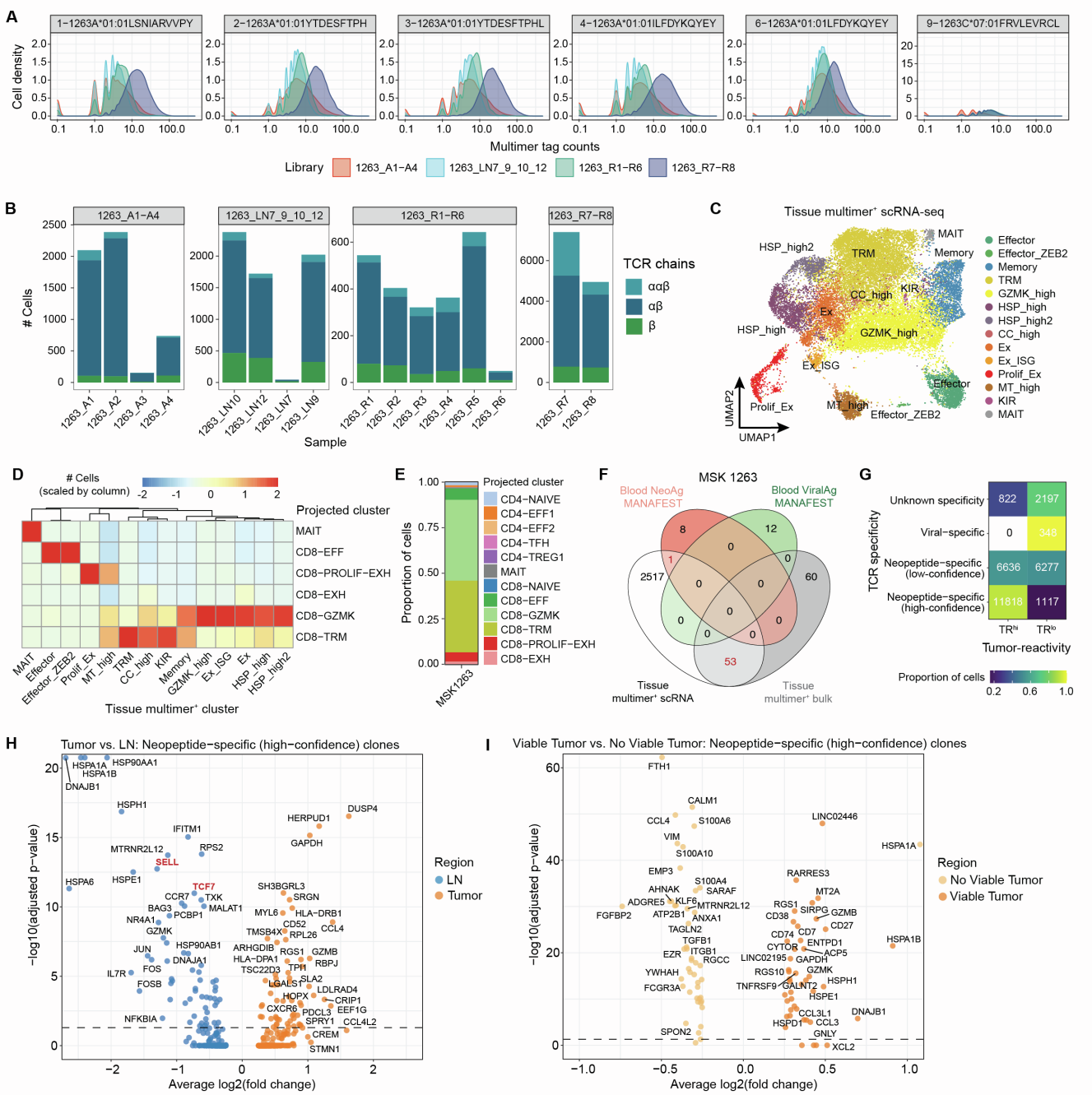

Figure S10. scRNA/TCR-seq of sorted neoantigen peptide multimer⁺ CD8⁺ T cells. Related to Figures 3 and 4.

A) Histograms of barcoded multimer tag counts in each sequenced multimer⁺ CD8⁺ T cell scRNA/TCR-seq library.

B) Bar plot of absolute number of sorted multimer⁺ CD8⁺ T cells for which TCRβ only (green) or both TCRα and TCRβ chains (teal) were reconstructed per regional sample undergoing scRNA/TCR-seq.

C) UMAP of cell clusters obtained from scRNA/TCR-seq of sorted multimer⁺ CD8⁺ T cells from MSK 1263.

D) Phenotype cluster concordance of clusters from tissue multimer⁺ CD8⁺ T dataset (query dataset, columns) and clusters from the tissue CD3⁺ scRNA/TCR-seq dataset (reference dataset, rows) for cells after label transfer from the reference. Heatmap values are scaled per tissue multimer⁺ cluster.

E) Projected phenotypes of cells in the tissue multimer$^+$ scRNA/TCR-seq dataset.
F) Venn diagram of overlap between TCRβ sequences from MSK 1263 identified by empirical TCR specificity methods. Numbers indicate the number of TCRβ sequences. Numbers in red represent TCRβ clones identified as neoantigen-specific by at least two empirical methods (designated as high-confidence neopeptide-specific clones).
G) Concordance of empirical antigen specificity and transcriptional tumor-reactivity category per cell in the tissue CD3$^+$ scRNA/TCR-seq dataset. Tiles are colored by the proportion of cells within each TCR specificity.
H) Volcano plot of differentially expressed genes between clone-matched cells in the LN and tumor from high-confidence neopeptide-specific CD8$^+$ T cell clones.
I) Volcano plot of differentially expressed genes between clone-matched cells in regions with and without viable tumor from high-confidence neopeptide-specific CD8$^+$ T cell clones.

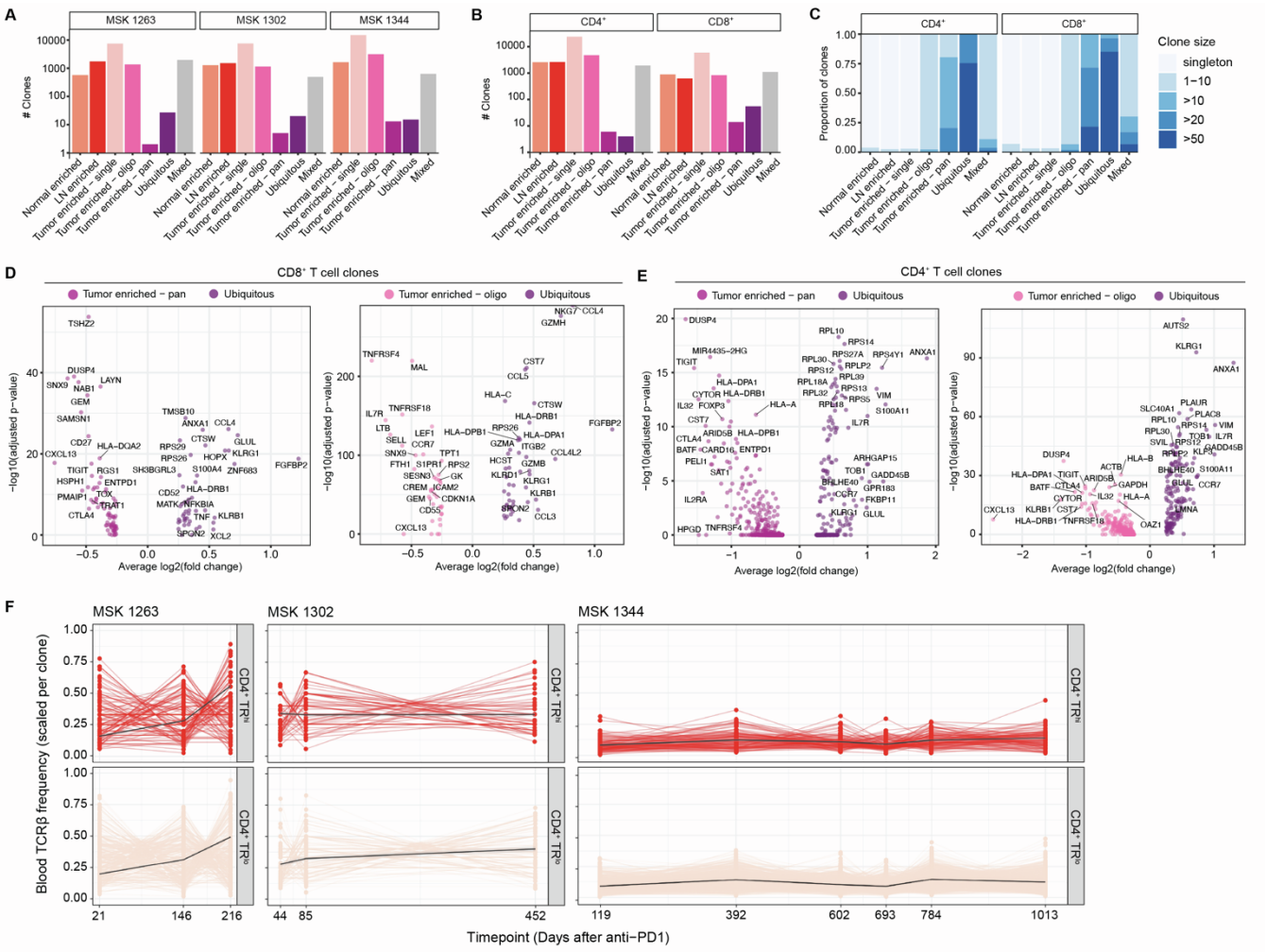

Figure S11. Regional patterns and peripheral persistence of TCR clones. Related to Figures 3 and 4.

A-B) Bar plot of the number of clones within each non-overlapping TCR regional pattern per patient (A) and per clone type among all patients (B).

C) Bar plots of the proportion of clones with the indicated clone sizes per TCR regional pattern of CD4$^+$ and CD8$^+$ T cell clones among all patients.

D-E) Volcano plot of differentially expressed genes between clones in the tumor enriched – pan (left) or tumor enriched – oligo (right) categories compared to ubiquitous clones among CD8$^+$ (D) or CD4$^+$ (E) T cell clones.

F) Circulating frequency over time of TR^{hi} (top) and TR^{lo} (bottom) CD4$^+$ clones from patients MSK 1263, MSK 1302, and MSK 1344.